Nanoscale Res Lett (2007) 2:161–167
DOI 10.1007/s11671-007-9048-6

NANO EXPRESS

Ultra violet sensors based on nanostructured ZnO spheres in network of nanowires: a novel approach

S. S. Hullavarad · N. V. Hullavarad · P. C. Karulkar · A. Luykx · P. Valdivia

Published online: 3 March 2007
© to the authors 2007

Abstract The ZnO nanostructures consisting of micro spheres in a network of nano wires were synthesized by direct vapor phase method. X-ray Photoelectron Spectroscopy measurements were carried out to understand the chemical nature of the sample. ZnO nanostructures exhibited band edge luminescence at 383 nm. The nanostructure based ZnO thin films were used to fabricate UV sensors. The photoresponse measurements were carried out and the responsivity was measured to be 50 mA W^{-1}. The rise and decay time measurements were also measured.

Keywords UV Sensor · Nano structures · Microspheres · Nanowire network · Rise/Decay time · Photoresponse · Photoluminescence

Introduction

Zinc oxide (ZnO) is a promising wide bandgap semiconductor for applications in ultra violet (UV) light emitting devices and sensors [1]. ZnO is a direct bandgap (Eg = 3.37 eV) semiconductor with a large exciton binding energy (60 meV) [2], exhibiting near UV emission, transparent conductivity [3] and piezoelectricity [4]. The high exciton binding energy in ZnO crystal can ensure an efficient excitonic emission at room temperature under low excitation intensity, which has potential applications in high efficiency light emitting diodes and UV lasers. ZnO has been widely reported as a visible blind UV sensor [5] over a wide range of applications in military and non-military arenas [6] that includes missile plume detection for hostile missile tracking, flame sensors, UV source monitoring, and calibration [7]. The research in the sensor area has lead many researchers to explore the possibility of widening the band gap of ZnO by alloying with Cd [8] and Mg so as to cover UV-A, UV-B and UV-C region of ultra violet region [9]. ZnO possess unique figures of merit, such as low thin-film growth temperatures (100–750 °C) [10], and radiation hardness [11], which are crucial for practical optoelectronic devices. Despite the challenges of reliable *p*-type doping in ZnO, there have been reports on fabrication of photodetectors [12], quantum wells[13], and superlattices [14] based on ZnO. As was predicted [15], the observation of room-temperature UV lasing from the ordered, nano-sized ZnO crystals provides an important step for the development of practical blue-UV laser. Thus, ZnO nanoscale structures such as one-dimension nanowires are attracting more attention because of their enormous potential as fundamental building blocks for nanoscale electronic [16] and photonic devices due to enhanced sensitivity offered by quantum confinement effects [17]. The sensors consisting of nanostructures [18] with large surface area to volume ratio (spheres) have better response characteristics and higher sensitivity [19]. ZnO nanostructured thin films consisting of spheres of diameter approximately 40–65 nm prepared by sol–gel dip coating method for gas sensing applications have been reported [20]. Zhang et al. [21], have

S. S. Hullavarad (✉) · N. V. Hullavarad · P. C. Karulkar
Office of Electronic Miniaturization, University of Alaska Fairbanks, Fairbanks, AK 99701, USA
e-mail: fnssh1@uaf.edu

A. Luykx · P. Valdivia
Center for Superconductivity Research, University of Maryland, College Park, MD 20742, USA

reported the fabrication of humidity sensors based on ZnO nanorods and nanowires grown by vapor phase transport process on pre patterned platinum electrode substrates. The formation of different shapes of nanostructures depends largely on temperature, pressure, heating/cooling rates and the saturation of reactive elements in the gaseous phase during the reaction. There have been reports on fabrication of complex ZnO structures with morphology like mushroom [22], spheres [23], ellipsoids, flowers and propellers [24]. Luo et al. [25] have reported the fabrication of UV photodiode by forming a heterojunction of *n*-ZnO nanowires of diameter (70–120 nm) with p-type Si. The authors have observed the UV responsivity of 70 mA W^{-1} under UV illumination of 365 nm at unusually higher (20 V) reverse bias. In this paper, we report the fabrication of ZnO UV sensor consisting of ZnO micro spheres in a matrix of nanowires.

Experimental

ZnO sheets consisting of spheres in nanowires were synthesized in a horizontal tube furnace (Lindberg) by a self catalyst Direct Vapor Phase (DVP) technique. Figure 1 shows the schematic of the growth set up. The source material Zn (99.9%) in granular form was placed at the center of the furnace (800 °C, heating rate 10 °C min^{-1}). Double side polished Al_2O_3 (0001) samples were used as substrates for optical characterization. In the initial stage, the furnace was flushed by Ar gas and was latter stabilized with a flow rate of 40–50 sccm. When the furnace reaches 420 °C, the Zn metal evaporates and O_2 gas was introduced with the combined gas mixture of 60 sccm. The evaporated Zn metal forms ZnO and was deposited on the Al_2O_3 substrates and also on the walls of the tube furnace. The process was carried out for 90 minutes and samples were pulled out after furnace was cooled down to room temperature. ZnO nanostructures were characterized by Environmental Scanning Electron Microscopy (Electro Scan), and Photoluminescence (PL) measurements to monitor the morphology (Laser Science, Inc, Model VSL-337 ND-S, 337 nm, 6 mW and Ocean Optics SD5000 spectrometer) and the band gap. Sensors were fabricated on a glass plate with silver conducting paste contacts with varying gaps in the range of 80–250 μm. The photo response measurements were carried out using Xe arc lamp, Thermo Oriel monochromator set up and a commercial UV sensor read out by Solartech, Inc. The experimental set up was calibrated with standard SiC and AlGaN UV detectors and the output power of the Xe arc lamp was measured by Newport standard power meter. The X-ray Photoelectron Spectroscopic (XPS) measurements were performed using Kratos Axis 165 spectrometer at a vacuum of 4×10^{-10} Torr with non-monochromatic Mg $K\alpha$ radiation. All binding-energies were calibrated with respect to C 1*s* at 284.6 eV.

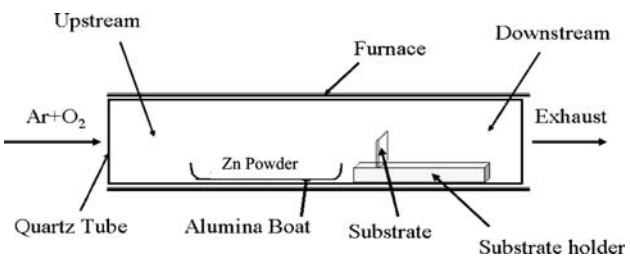

Fig. 1 Schematic showing the growth of ZnO nanostructures

Results and discussions

Figure 2 shows the photograph of flexible sheets of ZnO which were used for UV sensor fabrication. SEM images in Fig. 3(a) and (b) show the morphology of the ZnO films. The films contain micro spheres in the range of 600 nm–2 μm embedded in the network of intricate nanowires. The enlarged images in Fig. 3(c) and (d) reveal the network of nanowires that are 30–65 nm in diameter and a few microns in length. In an attempt to understand the process mechanism of formation of spheres alone in detail, we lowered the overall growth temperature from 800 °C to 600 °C (process temperature for the formation of ZnO microspheres in network of nanowires is 800 °C). Figure 4(a) and (b) show the SEM of low temperature

Fig. 2 The photograph of ZnO nanostructure film

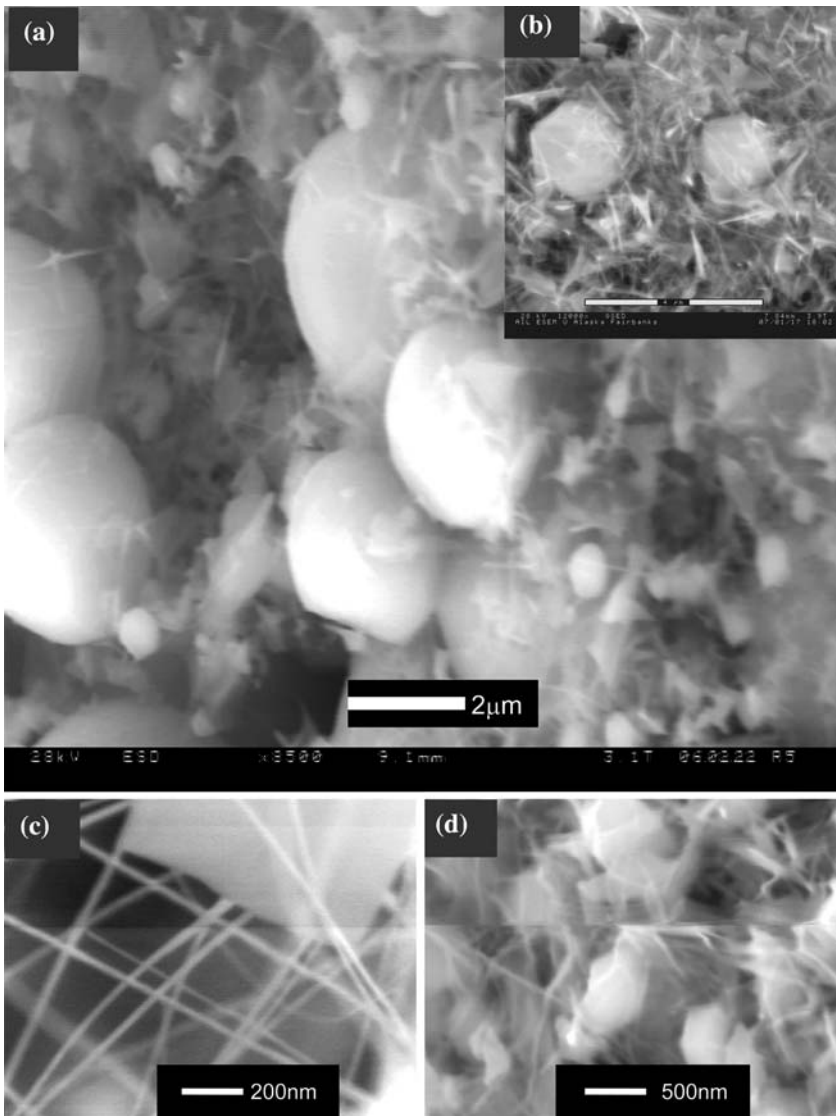

Fig. 3 SEM of the nanostructure ZnO thin film (**a**) and (**b**) micro spheres with a network of nanowires, (**c**) and (**d**) enlarged view of ZnO nanowires

processed ZnO in the identical set up. From the micrograph, it is evident that the size of sphere is around 2 μm (similar size as in Fig. 3(a)) before the spheres turn shaping into a perfect hexagon of size about 5 μm. The formation of radially spherical ZnO spheres at a lower growth temperature of 650 °C has been reported and the authors attempted to explain the evolution of spheres into nanorods when the samples were annealed to 1000 °C [26]. The radius of the spheres was calculated to be 400 nm from the formula proposed by Ding et al. [26];

$$r_{\min} = 2\sigma_{LV}V_L/RT\ln\sigma$$

where σ_{LV} is surface free energy of liquid–vapor, V_L is molar volume and σ is vapor phase supersaturation. The inflation of spheres continues with the process as more vapor gets condensed on to the small spheres. The mechanism for the formation of nanowires and spherical structure in a one step process (as observed in the present investigation) in the absence of any catalyst or a reducing agent is not very clear. However, we believe that complex nature of DVP process in which the rate of supersaturation of reactive elements varies, plays the key role in defining the shape and structure of the resulting material. Our experiments to understand the effect of gas kinetics in controlling the shapes are underway and can be found elsewhere (S. S. Hullavarad and P.C. Karulkar, under preparation). Mo et al. [27] have observed formation of ZnO nanorods embedded in micro hemispheres and spheres by hydrothermal-thermolysis of $Zn(en^{2+})$ in the presence of long chain polymer of—poly(sodium-4 styrenesulfonate)—(PSS) and the authors noted that such formation of multiple shapes is due to the presence of an appropriate amount of water soluble long chain polymer. In self catalyst

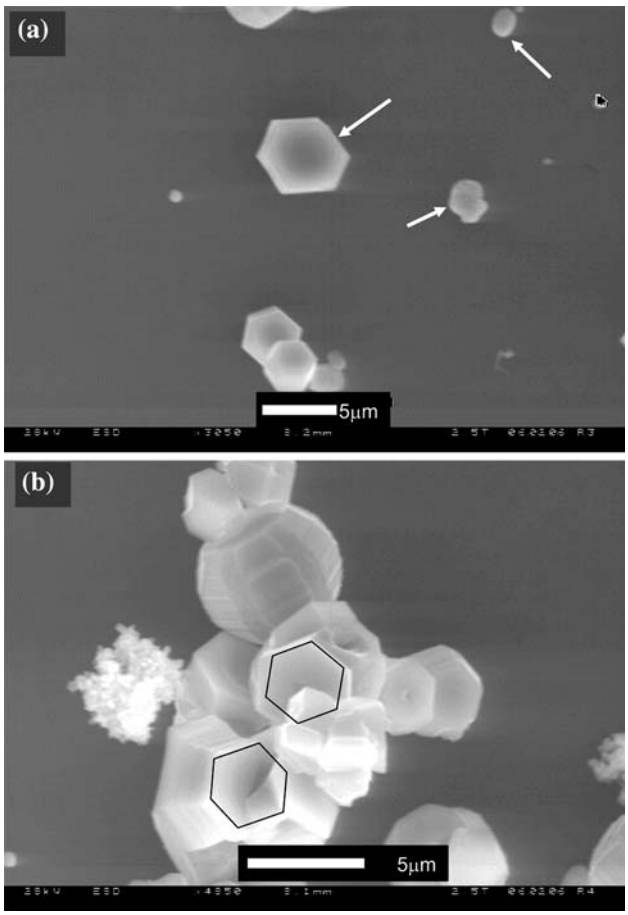

Fig. 4 (**a**) and (**b**) SEM of ZnO micro spheres evolving into hexagons

DVP technique, the supersaturation of reactive elements like Zn vapor and the oxygen favors the formation of nanowires and spheres like morphology. There have been reports [28] on the fabrication of ZnO nanowires of diameter 200 nm at a lower growth temperature of 650 °C and the reaction was carried out in N_2 atmosphere. The formation of nanowire or spheres or both of shapes in vapor phase depends on the temperature, carrier gas and the type of substrates. It is clear from the two experiments that the nature of carrier gas used in the vapor deposition process affects the shape of structures due to difference in masses of processing gases.

Figure 5 shows the XPS general scan spectrum for the ZnO nanostructure film consisting of nanowire and microspheres. The spectrum depicts the core levels at 90.3 eV and 531.5 eV corresponding to Zn 3p and O1s and Zn Auger lines Zn LMM b, c, d [29]. The ZnO thin films were investigated by the room temperature PL spectroscopy. The excitation energy of the laser was 3.6 eV corresponding to a wavelength of 340 nm. As

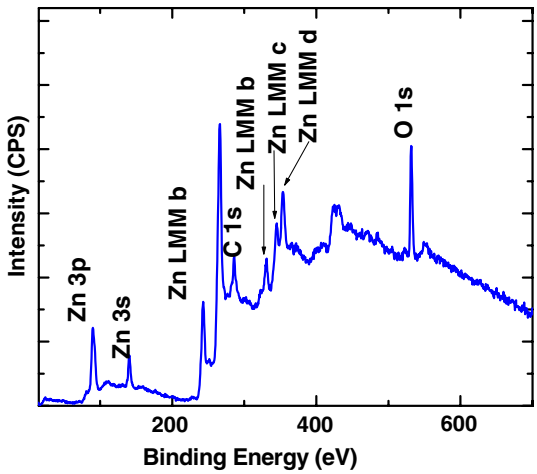

Fig. 5 XPS general scan of ZnO nanostructure consisting of microspheres and nanowires corresponding to morphology shown in Fig. 3

shown in Fig. 6, the dominant peak was observed at $\lambda = 383$ nm which is attributed to the recombination of free excitons through an exciton–exciton collision process (D^0X) corresponding to 3.2 eV [1]. The inset of Fig. 6 shows the bright blue/violet emission from the ZnO micro sphere-nanowires network film under laser illumination. The exciton peak has the full width at half maximum (FWHM) of 15 nm. Interestingly, the green emission at $\lambda = 512$ nm [30, 31] (2.41 eV) is absent in the PL spectrum indicating the absence of any non-stoichiometry between Zn and O [32–34].

The nanostructure ZnO film was pressed on to the silver conducting paste electrode with a defined gap (Fig. 7). The current–voltage characteristics were carried out with and without illumination as shown in Fig. 8. The dark (background) current of the nanostructure ZnO film device was 1×10^{-10} A at 1 V. This dark current is comparatively better than the thin film

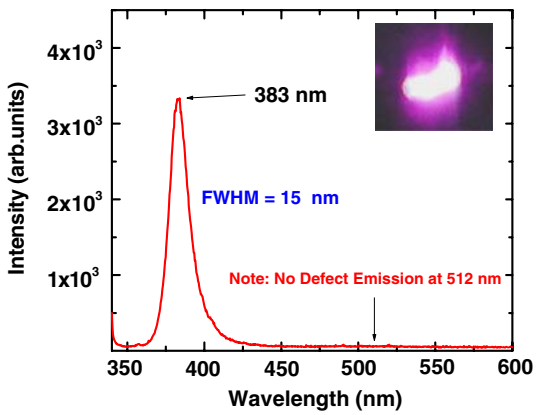

Fig. 6 PL spectrum of ZnO nanostructure thin film

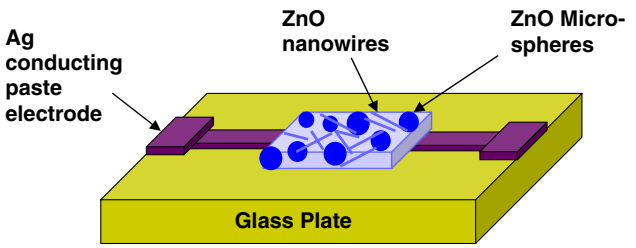

Fig. 7 The schematic of UV sensor formed from nanostructured ZnO thin film

based UV sensor fabricated from ZnO and MgZnO UV sensitive materials [35]. A lower dark current is desirable for a better sensor. When a ZnO nanowire is exposed to air, the negative space charge layer is created when the adsorbed oxygen molecule captures an electron from the conduction band and therefore the device exhibits higher resistivity. When the photon energy is larger than the band gap energy E_g, the incident radiation is absorbed in the ZnO nanostructured UV sensor, creating electron–hole pairs. The photogenerated, positively charged hole neutralizes the chemisorbed oxygen responsible for the higher resistance, increasing the conductivity of the device. As a consequence, the conductivity in the material increases, giving rise to photocurrent. The sensor exhibited a photo current of 1×10^{-8} A, at 1 V under UV illumination at 383 nm. The UV to Visible rejection ratio was found to be two orders of magnitude. The responsivity R of the UV sensor at 1 V corresponding to a dark current of 1×10^{-10} A was calculated to be 50 mA W^{-1} from the relation;

$$R = \frac{I_{Ph}}{P_{Op}}$$

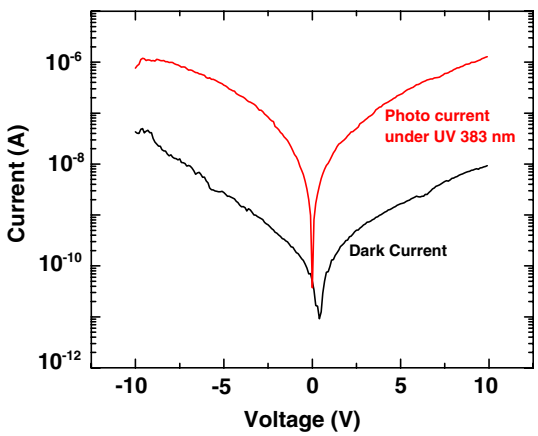

Fig. 8 *I–V* characteristics of ZnO UV sensor with and without UV illumination

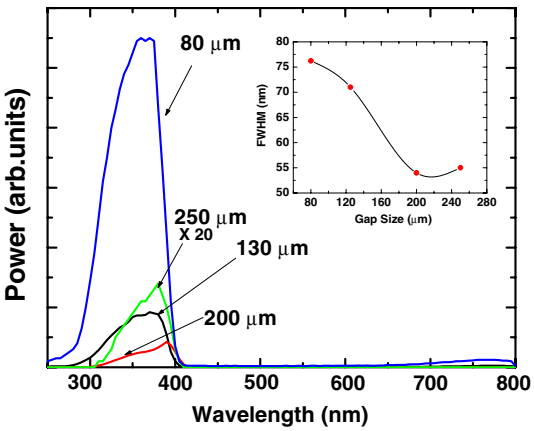

Fig 9 Photoresponse measurements of UV sensor as a function of electrode spacing. The inset shows the FWHM of photoresponse curves as a function of electrode spacing

where, the I_{Ph} is the photon induced current at $\lambda = 383$ nm with the power output P_{Op} is the incident optical power which was measured independently at the ZnO UV sensor location. Figure 9 shows the photo response measurements of nanostructure ZnO film device for varying electrode spacing of 80, 130, 200 and 250 μm. The response for the largest spacing of 250 microns is enhanced 20 times for clarity. The photo response signal output (mW/cm^2) was found to increase with the reducing electrode spacing. The full width at half maximum (FWHM) of the photo response curves are measured to be 76, 71, 54 and 55 nm for the electrode spacing of 80, 130, 200 and 250 μm, respectively. The effect of shapes and sizes of nanostructures on the photoresponse properties needs to be investigated and is seldom reported in the literature.

The device response in terms of rise and decay time at room atmosphere when the UV illumination turned

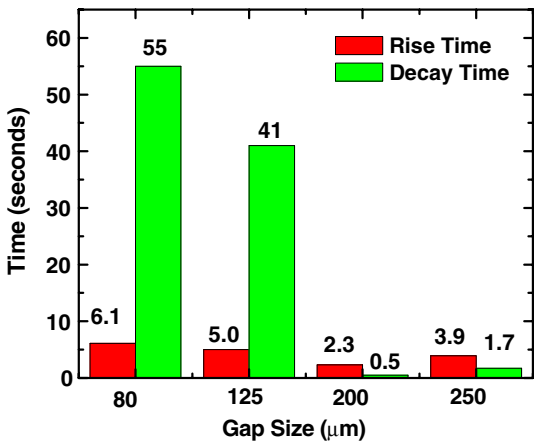

Fig. 10 The rise and decay time of UV sensor for different electrode spacing

ON and OFF was studied using a modified circuitry that involves a sensitive oscilloscope. Figure 10 shows the rise and decay time of ZnO micro sphere-nanowires network film device under UV illumination. The rise time was observed to be 6.1, 5, 2.3, 3.9 seconds while the decay time was observed to be 55, 41, 0.5 and 1.7 seconds for electrodes spacing of 80, 130, 200 and 250 μm, respectively. It is interesting to note that the rise and decay times are faster for the electrode spacing of 200 μm whereas the corresponding photo response was poor. Keem et al. [36] have studied the photo response of ZnO nanowires grown on pre-patterned Ti/Au electrodes with a spacing around 50 microns and measured photocurrents with the trapping time of electrons ranging from 10 ms to several hours through the nanowires excited by both the above and below gap light and concluded that the photo current is surface-related rather than bulk related. We believe that such faster rise and decay times observed in our photo response measurements result from the characteristic structure [37]. A comparative study of the effect of oxygen on UV sensors in the nano and the bulk regime is necessary to resolve the issues encountered in this study. The photoconductivity of ZnO and hence its response is known to depend on the presence of oxygen in the atmosphere [38]. It is interesting to study the effect of background oxygen pressure on the rise and decay time of the UV ZnO nanostructure sensor.

Conclusions

Fabrication of ZnO UV sensors are demonstrated by a simple route without employing the tedious clean room procedure of inter-digitized electrode formation. The active ZnO in the form of a flexible sheet consisted of micro spheres in a matrix of nanowires. The morphology of the deposited structures indicated that the sizes of ZnO nano-wires in the range of 30–65 nm and the micro spheres in the range of 600 nm–2 μm. The PL measurements indicated the exciton bandgap at 383 nm corresponding to band gap of 3.2 eV. The photoresponse measurements indicated that the multiple shapes involving the spheres in network of nanowires and the electrode spacing affect the sensor responsivity. This technique has a potential for scale up to fabricate UV sensors for mass production.

Acknowledgements SSH is thankful to Dr. Diane Pugel and Dr. R.D. Vispute for fruitful discussions. Authors would like to acknowledge the support from Defense Micro Electronic Agency (DMEA) at University of Alaska, Fairbanks.

References

1. U. Ozgur, Y.I. Alivov, C. Liu, A. Teke, M.A. Reshchikov, S. Do, S. Doan, V. Avrutin, S.-J. Cho, H. Morkoc, J. Appl. Phys. **98**, 041301 (2005)
2. Y.S. Park, C.W. Litton, T.C. Collins, D.C. Reynolds, Phys. Rev. **143**, 512 (1966)
3. D. Ravinder, J.K. Sharma, J. Appl. Phys. **58**, 838 (1985)
4. J. S. Wang, K.M. Lakin, Appl. Phys. Lett. **42**, 352 (1983)
5. G. Goncalves, A. Pimentel, E. Fortunato, R. Martins, E.L. Queiroz, R.F. Bianchi, R.M. Faria, J. Non-Crystalline Solids **352**, 1444 (2006)
6. http://www.mda.mil/mdalink/pdf/materials.pdf
7. http://gtresearchnews.gatech.edu/newsrelease/nanohelices.htm
8. T. Makino, Y. Segawa, M. Kawasaki, A. Ohtomo, R Shiroki, K. Tamura, T. Yasuda, H. Koinuma, Appl. Phys. Lett. **78**, 1237 (2001)
9. S.S. Hullavarad, S. Dhar, B. Varughese, I. Takeuchi, T. Venkatesan, R.D. Vispute, J. Vac. Sci. Technol. A **23**, 982 (2005)
10. S.J. Pearton, D.P. Norton, K. Ip, Y.W. Heo, T. Steiner, Prog. Mater. Sci. **50**, 293 (2005)
11. F.D. Auret, S.A. Goodman, M. Hayes, M.J. Legodi, H.A. van Laarhoven, D.C. Look, Appl. Phys. Lett. **79**, 3074 (2001)
12. S. Liang, H. Sheng, Y. Liu, Z. Huo, Y. Lu, H. Shen, J. Cryst. Growth **225**, 110 (2001)
13. T. Makino, A. Ohtomo, C.H. Chia, Y. Segawa, H. Koinuma, M. Kawasaki, Physica E: Low-dimensional Syst. Nanostruct. **21**, 671 (2004)
14. N.B. Chen, C.H. Sui, Mater. Sci. Eng. B, **126**, 16 (2006)
15. R.F. Service, Science **276**, 895 (1997)
16. M.H. Huang, S. Mao, H. Feick, H. Yan, Y. Wu, H. Kind, E. Weber, R. Russo, P. Yang, Science **292**, 1897 (2001)
17. N.I. Kovtyukhova, T.E. Mallouk, Chem. – Eur. J. **8**, 4354 (2002)
18. B. Liu, T. Ren, J. Zhang, H. Chen, J. Zhu, C. Burda, Electrochem. Commun. **9**, 551 (2007)
19. X.L. Cheng, H. Zhao, L.H. Huo, S. Gao, J.G. Zhao, Sensor Actuator B **102**, 248 (2004)
20. C. Ge, C. Xie, S. Cai, Mater. Sci. Eng. B, Doi:10.1016/j.mseb.2006.10.006 (2006)
21. Y. Zhang, K. Yu, D. Jiang, Z. Zhu, H. Geng, L. Luo, Appl. Surf. Sci. **242**, 212 (2005)
22. H. Wang, C. Xie, D. Zeng, Z. Yang, J. Colloid Interface Sci. DOI: yjcis 11765 (2006)
23. A. Umar, S.H. Kim, Y.H. Im, Y.B. Hahn, Superlattic. Microstruct. **39**, 238 (2006)
24. J. Liu, X. Huang, Y. Li, Q. Zhong, L. Ren, Mater. Lett. **60**, 1354 (2006)
25. L. Luo, Y. Zhang, S.S. Mao, L. Lin, Sensor Actuator A, 127, 2006, 201 (2005)
26. S. Ding, J. Guo, X. Yan, T. Lin, K. Xuan, J. Crystal Growth **284**, 142 (2005)
27. M. Mo., J.C. Yu, L. Zhang, S.A. Li, Adv Mater. **17**, 756 (2005)
28. A. Umar, S.H. Kim, Y.-S. Lee, K.S. Nahm, Y.B. Hahn, J. Crystal Growth **282**, 131 (2005)
29. C.D. Wagner, W.M. Riggs, L.E. Davis, J.F. Moulder, G.E. Mullenberg, *Handbook of X-ray Photoelectron Spectroscopy*, (Perkin-Elmer Corp., Eden Prairie, MN, USA, 1979)
30. B.S. Zou, R.B. Liu, F.F. Wang, A.L. Pan, L. Cao, Z.L. Wang, J. Phys. Chem. B **110**, 12865 (2006)
31. F. Leiter, H. Alves, D. Pfisterer, N.G. Romanov, D.M. Hofmann, B.K. Meyer, Physica B **340–342**, 201 (2003)

32. D. Banerjee, J.Y. Lao, D.Z. Wang, J.Y. Huang, Z.F. Ren, D. Steeves, B. Kimball, M. Sennett, Appl. Phys. Lett. **83**, 2061 (2003)
33. T.W. Kim, T. Kawazoe, S. Yamazaki, M. Ohtsu, T. Sekiguchi, Appl. Phys. Lett., **84**, 3358 (2004)
34. X. Wang, Q. Li, Z. Liu, J. Zhang, Z. Liu, R. Wang, Appl. Phys. Lett. **84**, 4941 (2004)
35. W. Yang, S.S. Hullavarad, B. Nagaraj, I. Takeuchi, R.P. Sharma, T. Venkatesan, R.D. Vispute, H. Shen, Appl. Phys. Lett. **82**, 3424 (2003)
36. K. Keem, H. Kim, G.T. Kim, J.S. Lee, B. Min, K. Cho, M.-Y. Sung, S. Kim, Appl. Phys. Lett. **84**, 4376 (2004)
37. S.E. Ahn, J.S. Lee, H. Kim, S. Kim, B.H. Kang, K.H. Kim, G.T. Kim, Appl. Phys. Lett. **84**, 5022 (2004)
38. Q.H. Li, Q. Wan, Y.X. Liang, T.H. Wang, Appl. Phys. Lett. **84**, 4556 (2004)